UNIVERSITÀ DEGLI STUDI DI PADOVA

DIPARTIMENTO DI INGEGNERIA INDUSTRIALE

CORSO DI LAUREA IN INGEGNERIA DEI MATERIALI

Tesi di Laurea Magistrale in Ingegneria dei Materiali

Hybrid-UV Direct Ink Writing of multicomponent glass

Relatrice: Dott.ssa Ing. Giorgia Franchin

Correlatrice: Dott.ssa Ing. Anna De Marzi

Laureanda: Giovanna Zaramella

Anno Accademico 2021-2022

To my grandma Erminia.

Abstract

The thesis focused on the *Additive Manufacturing* (AM) of two types of multi-component glass based on silica, one doped with cerium and the other with lanthanum, to increase respectively the photoluminescence and refractive index.

Mixtures with different quantities of silica and silica/precursor ratios were prepared and tested by analyzing their rheological properties. The compositions with pseudoplastic behavior were then selected and printed using a technology named Hybrid-UV Direct Ink Writing (DIW).

The samples thus obtained were then heat treated until complete sintering. Temperature and holding time have been modified in order to find a treatment suitable to obtain transparent components for both types of multi-component glass.

Finally, for silica-lanthanum glass, the increase in the refractive index was analyzed, while for silica-cerium glass, photoluminescence measurements were carried out.

Index

Index of tables

Index of figures

Chapter 1

Introduction

1.1 Glass

Glass has a lot of interesting properties such as hardness, transparency, thermal and chemical resistance (1). Silica glasses, in particular, are widely used and known for their extraordinary physico-chemical properties, such as resistance to the thermal shock, electrical properties, an excellent performance for light penetration, high resistance to deformation on heating and high chemical purity (2). Nevertheless, the final properties of silica glasses can be tailored by addition of metal oxides, thus allowing to tune their chemical durability (Al_2O_3), bioactivity (CaO, MgO), thermal resistance (B_2O_3) or optical properties (3). Specifically form this latter perspective, when the metal ions interact with the incident light, the glass will behave differently depending on the electric state of the oxides added.

Cerium, for example, enhances the photo-luminescence properties of silica glass: thanks to the 5d → 4f transitions of Ce^{3+} ions, when irradiated with UV light, it converts it into the visible range (λ=350 nm), thus emitting a blue light (4). Lanthanum, on the other side, is used to increase the refractive index and reduce the dispersion of the glass: its optical behavior depends on the phenomenon of absorption in the visible range and consequent transition in the orbital 4f of La^{3+} ions (5).

1.2 Manufacturing methods

Glass is one of the oldest materials known, dates to about 8000 BC. It originated in Phenicia and later was brought in Mesopotamia and in Egypt (6). From there, glass spread to Cyprus, Greece and in the Italian peninsula, especially in Venice (7). ‘Thousand flowers” glassmaking process is one of the first technique employed by these countries to produce open bakers and shallow dishes: in this process a shaped core was made to which section of colored glass canes were attached. The core and canes were replaced in an outer mold to keep the shape while the glass fused in an oven (8). After the mold and core removal, the glass surfaces would have been

smoothened. Another glassmaking process was to blow glass with a blowing iron: the latter was an iron tube about 1,5 meters, with a mouthpiece at one end and a knob for holding soft glass at the other end. A cluster of molten glass was collected on the knob and rolled in a suitable shape on a flat surface of iron called marver. The shape could be blown inside a mold or in air (8).

Nowadays, the two conventional ways to fabricate glass are lamination and blowing: the first is used to produce flat glass and the second to produce glass containers (9). Lamination consists in processing, through rollers, molten glass with consecutive steps of colling and annealing to remove any residual stresses. The current blowing reminds to the manual blowing of the ancients: the production begins with a small portion of glass (gob), obtained from the molten glass by gravity, which is inserted in a mold and then blown to make just a thin layer of glass to adhere to the mold surface, thus obtaining its shape (10). However, while such techniques have been widely investigated and used, they present some limitations: blowing, for example, depends on the shape of gob and molds, limiting the complexity of the geometries that can be fabricated; the same applies to lamination from which only glass sheets can be made (11).

Hence, to increase the complexity of the final glass component, more sophisticated production techniques have been developed, such as Additive Manufacturing techniques (AM).

1.2.1 Additive manufacturing

Additive manufacturing or 3D printing technologies allow the fabrication of freeform structures with high-resolution architectures of ceramic and glass materials. AM techniques allow to reduce waste of material and production time, thanks to their rapid prototyping characteristics (12). An example of AM techniques is Fused Deposition Modeling (FDM) (Figure 1.1) which printing process is based on the extrusion of a material in its molten state and its selective release on a building plate in a layer fashion. Materials for FDM must be thermoplastic in order to be partially fused and easily extruded out of tiny nozzles (i.e., 0.2÷0.8 mm) but then able to retain their filament shape upon cooling (13). A similar process has been also developed for the fabrication of glass: by using fusing deposition modeling, phosphate glasses with complex geometries were obtained. Specifically, glass filaments were fed through a heated extrusion nozzle in order to melt it and then deposit glass layer-by-layer (14) (Figure1.2). Such technique, however, presents some limitations in its field: FDM printers requires the material supply in the form of filament, and this involves difficulties to print 3D finely detailed items and finished product quality issues because during printing could appear lines between the printed layers (15).

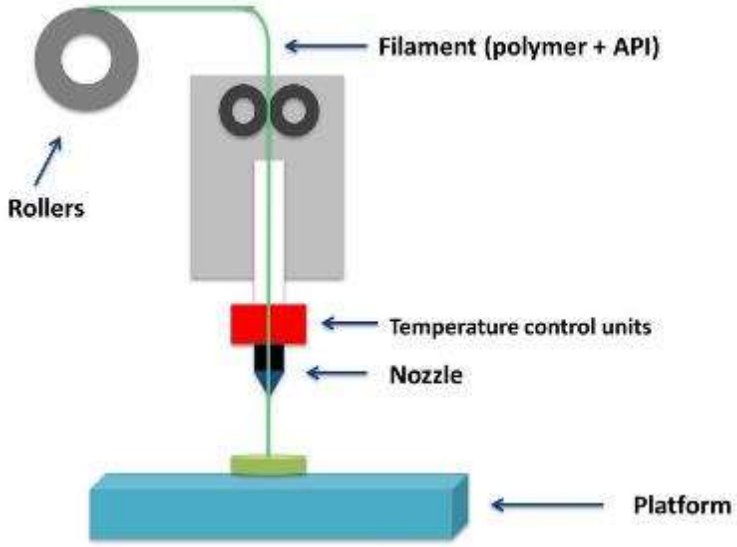

Figure 1.1. Schematic of FDM process (16).

Figure 1.2. FDM printer (17).

Other AM techniques that can be used in the fabrication of glass components are the Direct Ink Writing (DIW) (Figure 1.3) and the Vat-photopolymerization techniques. DIW process is similar to FDM: it is a layer-by-layer technique based on the extrusion of a material which, in this case, does not need to be heated to be extruded. Indeed, pseudoplastic inks must be used to

successfully print using this technique. Pseudoplastic materials show a decrease in their viscosity when the extrusion forces are applied, but a rapid increase when such forces are removed (i.e., out of the nozzle), favoring the filament solidification; common exploited phenomena include gelation, solvent evaporation, or temperature- induced phase change (18). Moreover, the ink must have an appropriate rheology after printing to prevent the stacked filaments from falling below their own weight (18).

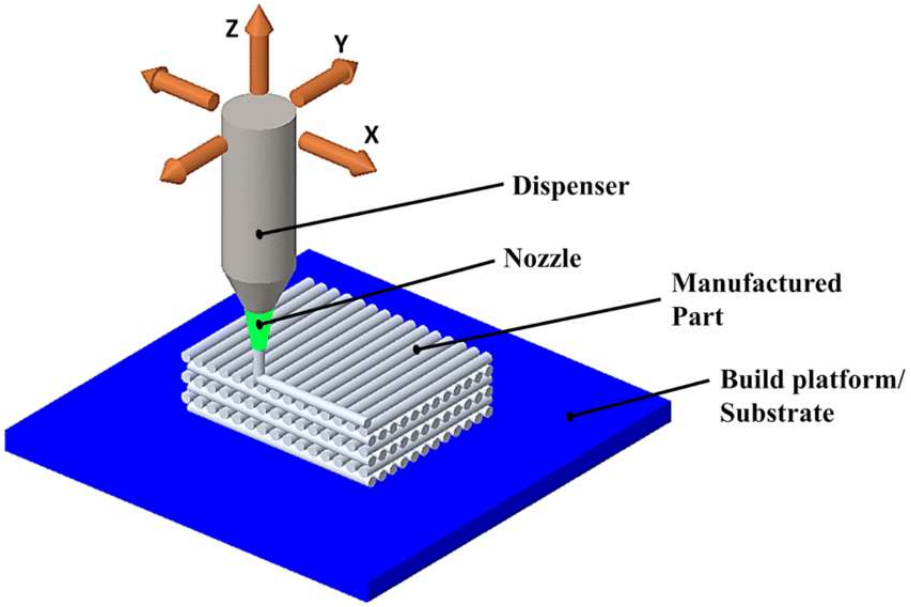

Figure 1.3. A schematic illustration of DIW (19).

DIW depends also on machine parameters as nozzle size, print speed and pressure: all such parameters influence the print accuracy and resolution. Particularly, a print resolution will be high, much more the diameters of the extruded filament approach the diameter of the nozzle (20).

DIW can be used to form silica green bodies of different shapes. By adding silica powder to a liquid system, a colloidal suspension is formed: attractive interactions can either arise from hydrogen bridges between hydrogen- and oxygen-containing moieties or from electrostatic forces between charged particles and bridging ions. When the ink yields under stress, the interparticle bonds are broken and large clusters of particles gain mobility. With increasing stress, the particle clusters are fragmented into smaller flocs, determining the shear-thinning behavior (21). Filament extruded using inks with a silica content retain their extruded shapes well (18).

Vat-photopolymerization techniques such as Digital Light Processing or Stereolithography (DLP and SLA, respectively), on the other hand, are based on the photopolymerization of an ink typically composed by a mixture of acrylates, a photo-initiator, and additives. It can be used

also in the production of ceramics: in this case, ceramic powders are dispersed inside the mixture (22). A schematic of a classic DLP machine is illustrated in Figure 1.3. In order to obtain the desired component, either the build plate or the vat containing the photo-curable ink move along the vertical axis, allowing the formation of a thin layer of material (50÷100 μm). A light source (usually in the UV-VIS range) is then used to project the layers composing the CAD model.

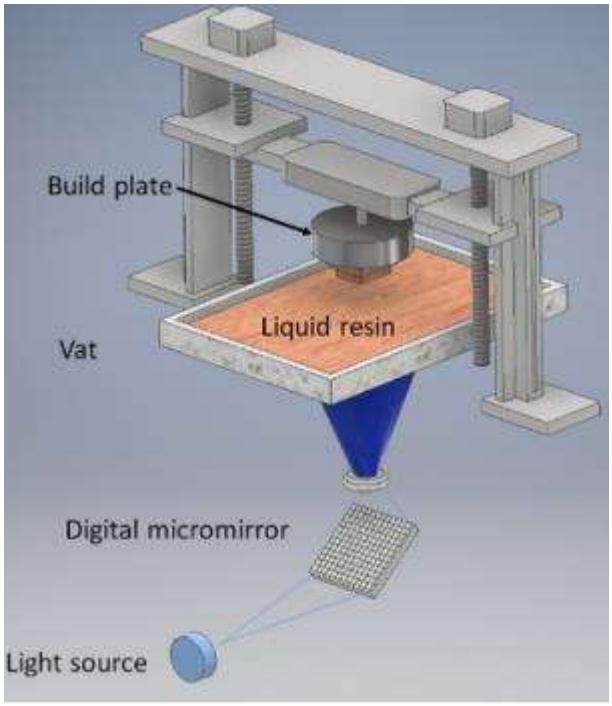

Figure 1.4. A schematic illustration of DLP system (23).

In this case, the requirements for a successful print are low viscosity inks with high reactivity to the UV light in order to allow faster printing process compared to DIW and fewer printing defects, like holes, due to a not uniform curing (24). Moreover, when DLP is employed with ceramic-based slurries, it should be considered the interaction existing between the incident light and the particles. Indeed, this leads to scattering and/or absorption phenomena of the UV light, consequently decreasing the curing depth, resolution, and rigidity of the printed sample. This should be avoided: by limiting the light, the polymerization process is delayed (20), therefore leading to an increase of the overall processing time.

Nevertheless, such phenomena can be partially avoided by matching the refractive indexes of the reagents. Specifically, by decreasing the difference between the refractive index of the ceramic particles and the one of the solvents (acrylates + additives), it is possible to increase the curing depth and avoid defects in the printed components (20). This is particularly

interesting in the fabrication of glass components since the refractive index of silica (1,458) can be matched by some acrylates, for example 2- Hydroxyethyl methacrylate HEMA (1,453).

This is the reason why a lot of works have been published related to the fabrication of glass components via DLP. Cai et al., for example, dispersed hydrophilic fumed silica, in different percentages, in a premix composed by acrylates, plasticizer and solvents; transparent 3D glass components were ultimately obtained (24). Nevertheless, this type of printing presents some limitations: because of its operating mechanism, generates a stair stepping effect on curved surfaces that limits the surface quality of the printed component; also, printed part dimensions depends on vat size: this can cause a limit in the size of printable components. (22)

1.2.2 Hybrid UV-DIW

As mentioned in the last paragraph, DIW inks have strict rheological requirements: other than a pseudoplastic behavior, they should possess an initial yield stress and a storage modulus (G') high enough for support-less structures to retain their shape with minimum deformation. DLP inks, instead, need to possess a low viscosity and an adequate reactivity to UV light.

In order to overcome such limitations, a new technique has been recently developed, which incorporates the mechanism of extrusion of DIW and a UV source, referred to as a hybrid-UV DIW technique (Figure 1.5)

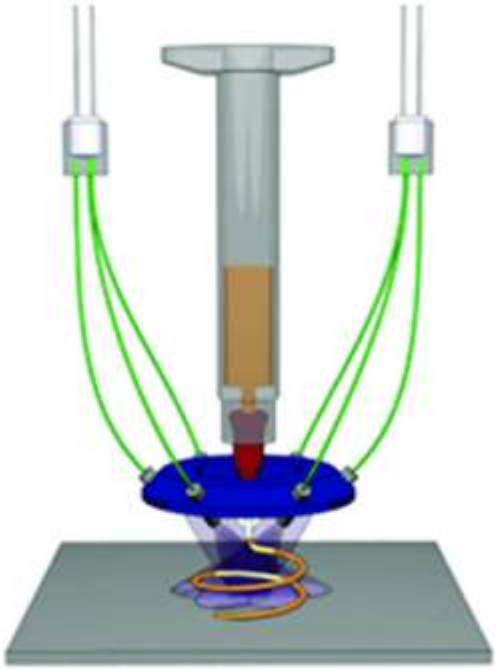

Figure 1.5. A schematic of the hybrid UV-DIW technique (25).

In this case, the printing process is based on the extrusion of a photocurable ink, which consolidates its shape after the exit from the nozzle thanks to the photo-polymerization process by exposition to a UV source. In this way, it is possible to obtain solid components having more complex shapes: thanks to the fast photo-crosslinking, the filament can maintain its shape not only along XY plane but also in the Z direction, allowing the realization of free-forming geometries (20). The UV-DIW technique will be used to print complex geometries; in addition, it has the advantages of high forming accuracy, good surface quality and fast forming speed which permits to obtain complex structures as required in optical field.

While such hybrid technique has been validated for the fabrication of mono-component silica-based glasses geometries, the goal of the present thesis project is the production of multicomponent silica-based glasses comprising cerium and lanthanum precursors.

Chapter 2

Experimental Procedure

In the following paragraphs the materials used, the method for inks preparation and printing, the heat treatment and characterization of samples will be described.

2.1 Materials

The formulation of multi-component glasses started from an already published photo-curable silica-based ink (20) composition at which metal-oxide precursors were added. Specifically, fumed silica particles (Aerosil OX50, Evonik Group, Germany) and tetraethyl orthosilicate (TEOS, Sigma- Aldrich, Germany) were chosen as the silica sources. Tetra (ethylene glycol) diacrylate (TEGDA, Sigma- Aldrich, Germany), 2- Hydroxyethyl methacrylate (HEMA, Sigma- Aldrich, Germany) and 2- Phenoxyethanol (POE, Sigma- Aldrich, Germany) were selected as the acrylates and the solvent, respectively, while bis (2, 4, 6-trimethyl benzoyl)-phenyl phosphine oxide (Omnirad 819, IGM Resins, Netherlands) acted as the photo-initiator.

Lanthanum (III) nitrate hydrate (Sigma Aldrich, Germany) and cerium (III) nitrate hexahydrate (Sigma Aldrich, Germany) were selected as the precursors due to their solubility in common organic solvents.

Different compositions were prepared for each of the precursors in order to obtain transparent multi-component samples, as shown in Table 2.1 and Table 2.2. Final oxides composition of the two glasses were $SiO_2 : Ce_2O_3 = 99.8 : 0.2$ and $SiO_2 : La_2O_3 = 91.2 : 8.8$.

Table 2.1. Different compositions for Cerium (III) Nitrate Hexahydrate ink.

Compositions [wt.%]	**1**	**2**	**3**	**4**
TEOS	24.92	25.15	25.15	24.57
HEMA	9.67	9.75	9.75	9.53
POE	3.80	3.84	3.84	3.75
TEGDA	24.71	24.38	24.39	23.80
OX 50	35.97	36.28	36.29	37.78
Ce precursor	0.98	0.12	0.10	0.10
OMNIRAD 819	0.48	0.49	0.49	0.47

Table 2.2. Different compositions for Lanthanum (III) Nitrate Hydrate ink.

Compositions [wt.%]	**1**	**2**	**3**	**4**	**5**
TEOS	23.71	34.24	28.14	28.14	26.16
HEMA	9.19	6.50	8.09	7.71	7.28
POE	3.62	2.57	3.18	3.04	2.85
TEGDA	22.98	16.28	20.14	19.26	18.18
OX50	34.20	34.24	34.21	35.62	40.91
La precursor	5.84	5.85	5.86	5.84	4.62
OMNIRAD 819	0.46	0.32	0.40	0.38	0.36

2.2 Ink preparation

The inks were obtained by firstly adding the precursor (previously manually ground with a mortar) to POE and then by mixing the solution in a planetary mixer (ARE-250, THINKY, Japan) for 2 min at 2000 rpm. Then HEMA and TEGDA are added. Silica powder was added in 9 steps (each step is followed by mixing for 2 min at 2000 rpm) in decreasing quantities so that the powder can be optimally dispersed in liquid reagents. Due to the extreme stresses applied to the mixture, the container of the ink used to heat up. For this reason, it was alternatively immersed in a water and ice bath in order to cool it down between subsequent mixing-addition steps. At last, TEOS and Omnirad 819 were added.

Later, the inks obtained were loaded into a UV-block syringe and subjected to the defoaming procedure in the planetary mixer (ARE-250, THINKY, Japan) to remove air bubbles trapped during the preparation of the mixture.

2.3 Hybrid UV setup and printing process

A custom-made UV-DIW setup was used (20). Specifically, it was composed by a hexagonal ring, at which micro-LEDs spotlights (395-400 nm, 10-15 lumen) are attached. This is then connected to 3D printer (Figure 2.1) (Delta 2040 Turbo 2, WASP, Italy). A 30 mL UV-block syringe and the nozzle tip attached to it (Vieweg GmbH, Germany) were then placed so that the nozzle would be in the center of the hexagonal ring (Figure 2.2). The extrusion process was controlled by means of an air pressure digital dispenser (DC 307, Vieweg GmbH, Germany). In order to prevent cross-linking of the ink on the nozzle end, therefore causing its clogging, a cylindrical lid was used to cover the nozzle.

Figure 2.1. Image of 3D printer, Delta Turbo 2, WASP with the hybrid setup installed.

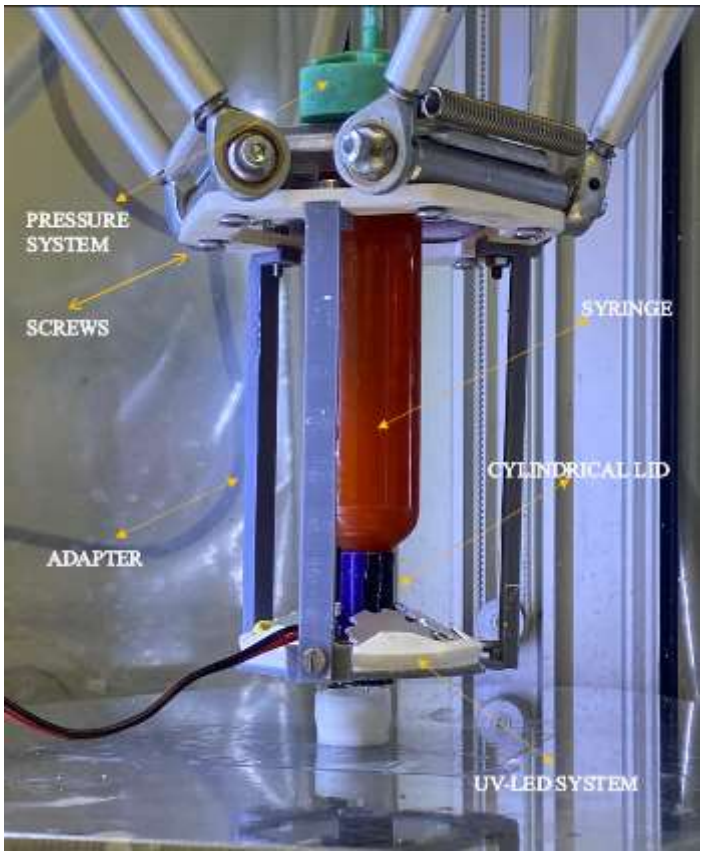

Figure 2.2. A schematic illustration of Hybrid UV-DIW components.

The UV-LEDs ring has an intensity of 6 mW cm^{-2} and is powered with a 24V – 10A power supply unit. The digital models are designed with Rhino 3D modelling software (2020, Rhinoceros 6, Robert Mc Neel & Associates, USA). (20)

During printing it is important to control print speed and pressure: if the printing speed is too high, the ink filament can break, while if the applied pressure is too low the filament cannot be extruded. For the two different precursors, these two parameters are different, while the nozzle tip is the same. (Table 2.3)

After printing, the printed samples were ready for debinding treatment and for sintering.

Table 2.3. Print speed, pressure, and nozzle tip dimeter for each ink.

Type of ink	Print speed [mm/s]	Pressure [bar]	Nozzle tip diameter [µm]
Ce-based	7	1,2	580
La-based	10	0,4	580

2.4 Ink characterization

A rotational rheometer (Kinexus Lab +, Netzsch, Germany) (Figure 2.3 (a)) was used to analyze the rheological behavior of the inks. The shear stress and viscosity were measured as a function of the shear rate between 0.1-500 s^{-1} with a 1°/40 mm cone-plate geometry with a gap of 0,03 mm.

In order to assess the reactivity of the ink upon irradiation, a UV plate system accessory (KNXF007, Netzsch, Germany), composed by a 40 mW cm^{-2} UV lamp (Figure 2.3 (b)) (Omnicure series 2000, Excelitas Technologies, United States) was utilized for photorheological characterization using an 8 mm parallel geometry and a 0,2 mm and 0,05 mm gap for cerium and lanthanum based inks, respectively. A three-step profile test was performed to consider the evolution of shear viscosity, composed of: a) in the first step the shear stress was not applied, b) the shear stress was applied after 10 s from the first step, c) the shear stress

was removed after 20s from the second step; the test was repeated both with the UV lamp turned off and on during the last step.

(a)  (b) 

Figure 2.3. Rheometer (a) and UV lamp (b).

2.5 Heating treatments

Heat treatments are divided into two phases: the first comprises debinding, during which the organic part of samples degrades, whereas the second is the sintering phase.

Debinding was performed into an oven (BRF14/5, Elite Thermal Systems Ltd, England) following this program reported in the table 2.4 (20) After this step, brown bodies were ready for sintering treatment which was performed in a bottom loading furnace (LHT 01/07 LB Speed, Nabertherm GmbH, Germany), at two different temperatures and for different holding times in order to find a treatment able to give transparent samples, as reported in the Table 2.3. The treatment was followed up by a rapid cooling thanks to the opening, at the sintering temperature, and the descent of platform oven on which the samples were placed.

Table 2.4: Debinding parameters.

Heat treatment	Temperature (°C)	Heating Rate (°C/min)	Holding Time (h)
Debinding	160	0.5	1
	200	0.5	1
	350	0.5	1
	800	2	1

Table 2.5. Temperatures and times of sintering.

Temperatures [°C]	**Holding time [min]**
1350	15
	30
	60
1400	5
	10
	15

2.6 Glass characterization

2.6.1 Porosity and density measurements

For porosity measurements, the Archimedes method was used. By following such method, apparent porosity (%AP) and density (ASG) can be measured. For each sample, soaked weight, dry weight and suspended weight are measured following (26):

$$\%AP = \frac{(Soaked\ weight - Dry\ weight\ ) * 100}{(Soaked\ weight - Suspended\ weight)} \quad (1)$$

$$ASG = \frac{(Dry\ weight\ )}{(Dry\ weight - Suspended\ weight)}. \quad (2)$$

2.6.2 Surface analysis

Images of the post-sintering samples were taken with an optical microscope (Stemi 2000-C, Carl Zeiss, Germany) using a zoom range of 0,65x-5.0x.

2.6.3 Photoluminescence

Cerium, as reported in the paragraph §1.1, has photoluminescence properties: absorbance spectra in the UV-VIS range was collected using a spectrophotometer (V-570, Jasko, United States) (Figure 2.4). The measurements were carried out with a bandwidth of 2,5 nm.

2.6.4 Refractive Index

Refractive index measurements on transparent lanthanum-based glasses were performed using a refractometer (2WAJ, Optika Microscopes, Italy) (Figure 2.5). To do so, sintered components having dimensions 20x10x1 mm were polished to obtain a flat surface that was later analyzed.

Figure 2.4. Refractometer 2WAJ.

Chapter 3

Results and discussion

This chapter focuses on analyzing the data obtained starting from ink optimization, heat treatments, density and porosity measurements, rheology analysis, hybrid UV printing process and optical measurements.

3.1 Ink Optimization

As reported in the paragraph §1.1, an ink suitable for hybrid-UV DIW printing should have a shear thinning behavior to be easily extrudable through the extrusion nozzle and reactive to UV light in such a way to create support-less features.

For the preparation of multicomponent inks, a silica-based mixture (mono-component) was used: silica is given not only by fumed silica but also by TEOS which makes the inks suitable for extrusion (20). Also, TEGDA and HEMA are present in silica-based ink as photo-curable components and were selected for their refractive indexes which are close to that of fumed silica. The coincidence of refractive indices (HEMA=1.453 and TEGDA=1.457) reduces the scattering phenomena, which would lead to a lower penetration depth of UV radiation and permits to obtain a well-dispersed and loaded ink without greatly increasing the viscosity (20). However, HEMA and TEOS have some differences in the number and type of functional groups: HEMA has only one vinyl group and two hydroxyl groups which makes it more suitable to form a solvation layer around fumed silica particle surface, while TEGDA has two vinyl groups which permits it to cure faster than HEMA. Therefore, by increasing the amount of TEGDA in respect of HEMA, the particle-liquid interactions can be reduced which make ink more viscous due to particle-particle interaction. The weight ratio of HEMA/TEGDA is 2.5 which gives the right compromise between rheological properties and curing speed (20).

Another important step is the addition of precursors to one-component system: due to the difference in particles diameters between the particles of the latter, respectively lanthanum (III) nitrate hydrate and cerium (III) nitrate hexahydrate, and those of fumed silica and to their

different solubility and dispersion is difficult to introduce these oxides formers in the silica-based mixture. Specifically, the nitrate salts chosen are soluble in water, acid solution or alcohols. Both water and acid solutions, however, due to -OH group can solvate further the silica powder by decreasing viscosity and compromising rheology of the final ink. Therefore, both precursors were firstly dispersed in 2-phenoxyethanol (POE). POE is also a solvent for silica particles thanks to its hydroxyl groups, thus creating the solvated layer around silica particles. In addition, it has a high boiling point which helps in maintaining inks stable at room temperature. Its only problem is that it has a different refractive index (1.534) than the other reagents and so its amount must be limited to avoid the reduction of curing depth, as reported before. Therefore, a ratio of HEMA/POE equal to 2.6 was selected (20).

A similar problem in the refractive index matching exists for the precursors, since the one of Lanthanum (III) nitrate hydrate is 1.449, while the one of Cerium (III) Nitrate Hexahydrate is 1.529 (27). Therefore, the ratio of silica oxides/precursor oxides that gives the right compromise between improving the optical properties of silica-based glass an optimizing the ink from a rheological point of view is, respectively for Lanthanum Nitrate and Cerium Nitrate, 91.2: 8.8 and 99.2:0.8.

As reported above, TEOS is added at the end of ink preparation. TEOS does not have hydroxyl groups which permit silica solvation, unlike HEMA which on the contrary increases the particles-liquid interaction by making ink less viscous. Precisely because of HEMA action, the particle-particle affinity is reduced by inhibiting the formation of a network (Figure 3.1 a): TEOS, if added in the right quantities, being a stearic agent, it limits particle-liquid interaction by remaining confined between silica particles (Figure 3.1 b). If inks were only of silica powder, shear thinning behavior would be up to critical shear rate value and then vary to a shear thickening or dilatant behavior, in which viscosity increases when shear rate increases. (20)

Figure 3.1. (a) Effect of silica solvation by HEMA; (b) TEOS effect on ink.

3.2 Rheological analysis

The mixtures from which transparent samples are obtained have been analyzed to verify that they meet the requirements for a hybrid-UV direct ink writing printing.

3.2.1 Pseudoplastic behavior assessment

As reported in paragraph §1.2, ink must have a pseudoplastic behavior in which viscosity decreases when shear rate increases by following a power law model (28):

$$\sigma = K\,\gamma^{n} \tag{3}$$

where σ and γ represents the shear stress and the shear rate, while K and n represent consistency index and the power of the fluid equation. The maximum shear rate at the nozzle walls can be obtained from Newtonian fluids equation corrected by Rabinovitch equation:

$$\gamma_{wall} = \frac{4Q}{\pi r^{3}}\left(\frac{3n+1}{4n}\right) \tag{4}$$

where Q and r represent the flow rate and the radius of nozzle end. From image 3.2 and 3.3 both cerium nitrate and lanthanum nitrate inks have a shear thinning behavior.

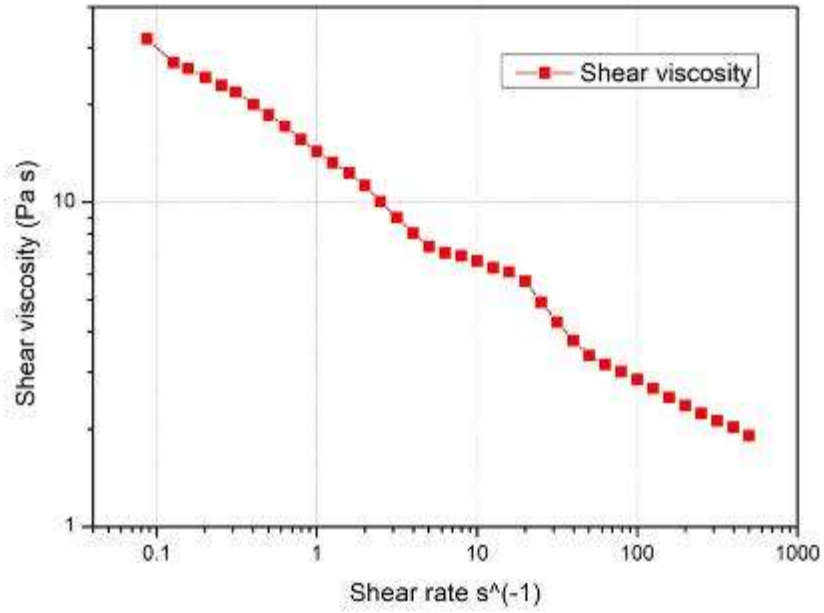

Figure 3.2. Shear thinning behavior of composition 4 of cerium nitrate ink.

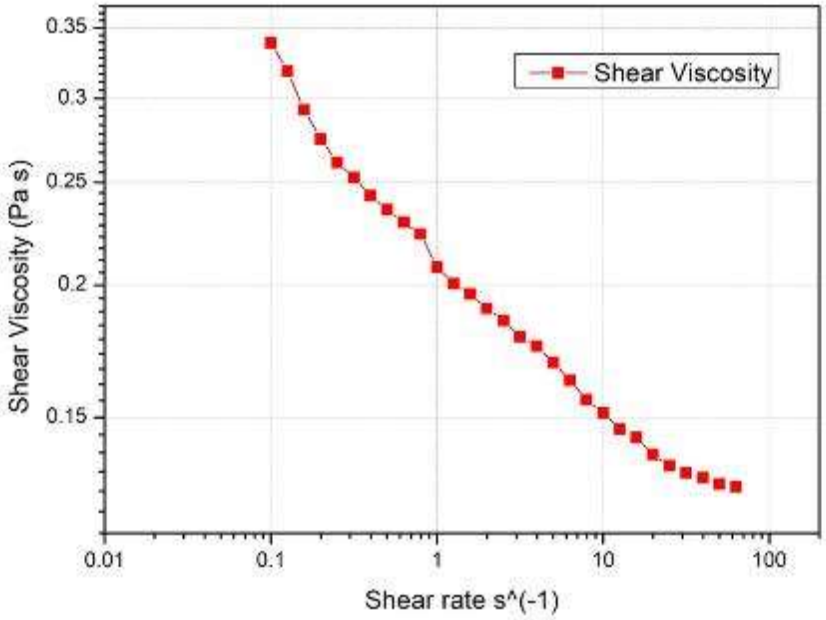

Figure 3.3. Shear thinning behavior of composition 5 of lanthanum nitrate ink.

Thanks to the addition of TEOS to the inks, the behavior assumes this linear trend in which viscosity decreases when shear rate increases (see paragraph §3.1): TEOS minimizes liquid-silica particle interaction, limiting the shear thickening effect that would occur for high shear

rate. This behavior is due to solvation of silica particles by HEMA which limits the formation of a stable network and so inks would be unsuitable for hybrid printing. (20)

Another fundamental detail visible from the graphs is the substantial difference in viscosity between the two inks, which is higher for the cerium (1-12 Pa s) and lower for lanthanum (0.1-0.35 Pa s): in fact, during printing, component characterized by several overlapping layers was obtained from cerium ink, while from lanthanum ink a single layer component which indicates that the low viscosity has negatively affected the printing of more complex structures.

3.1.1 Three steps profile measurements

The rheological behavior of inks being irradiated by UV light was measured by testing shear viscosity evolution over time during three steps profile test: this three steps test reproduces what would happen during the printing process. The first step represents the inks before extrusion inside syringe in low shear condition; the second phase describes high shear conditions occurring during ink extrusion, and the third phase simulates the ink after extrusion (20). For lanthanum ink and for cerium ink, the test was performed in two different conditions: (a) with UV light turned off during the third phase, and (b) with UV light turned on for 10s during the third phase.

For the Cerium (III) Nitrate Hexahydrate Ink (Figure 3.4) the viscosity, in the third phase, returns immediately to be the same as that of the first phase ($\sim 5 * 10^2 Pa\ s$), a value that should allow the filament to maintain its shape to some extent when deposited. However, when UV-light is turned on, the viscosity increases considerably compared to the first phase ($\sim 10^6\ Pa\ s$). This means that, by turning on the UV light during printing, the filament can solidify quickly to high rigidity, allowing to obtain a self-supporting component.

For the Lanthanum (III) Nitrate Hexahydrate Ink (Figure 3.5) the viscosity, in the third phase with UV light turned off, remains slightly lower ($\sim$ 5 Pa s) than the value of the first phase and definitely lower than the previous ink: this results in difficulties during printing to obtain complex prints compared to the cerium ink. By turning on UV lights, the filament could retain its shape thanks to the rapid increase of the ink viscosity to $\sim 10^6\ Pa\ s$.

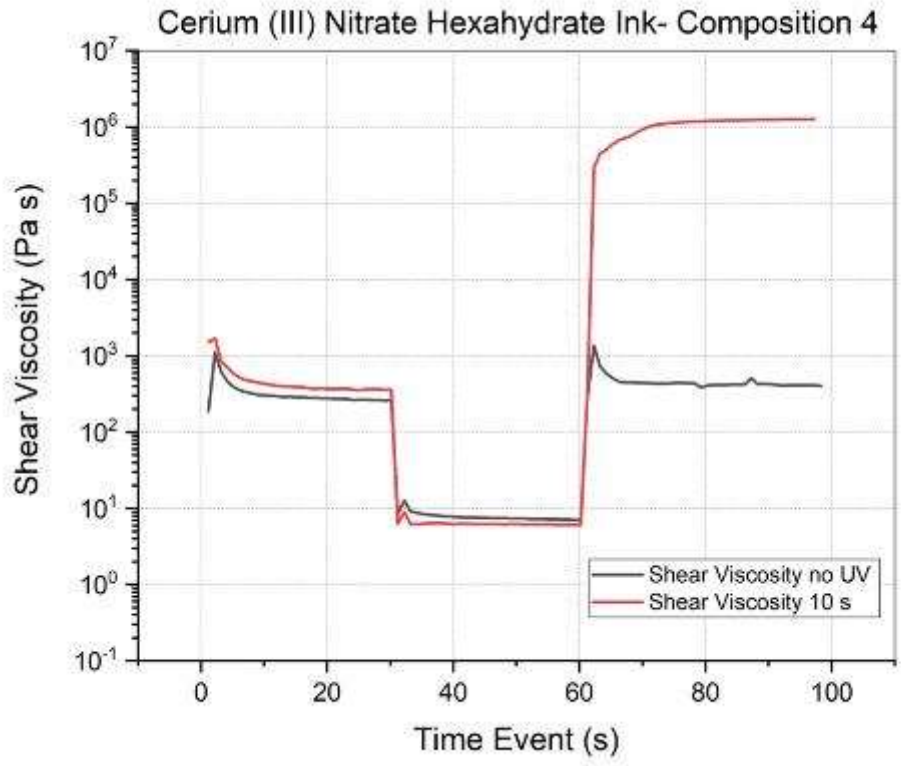

Figure 3.4. Three steps profile test for composition 4 of cerium nitrate ink.

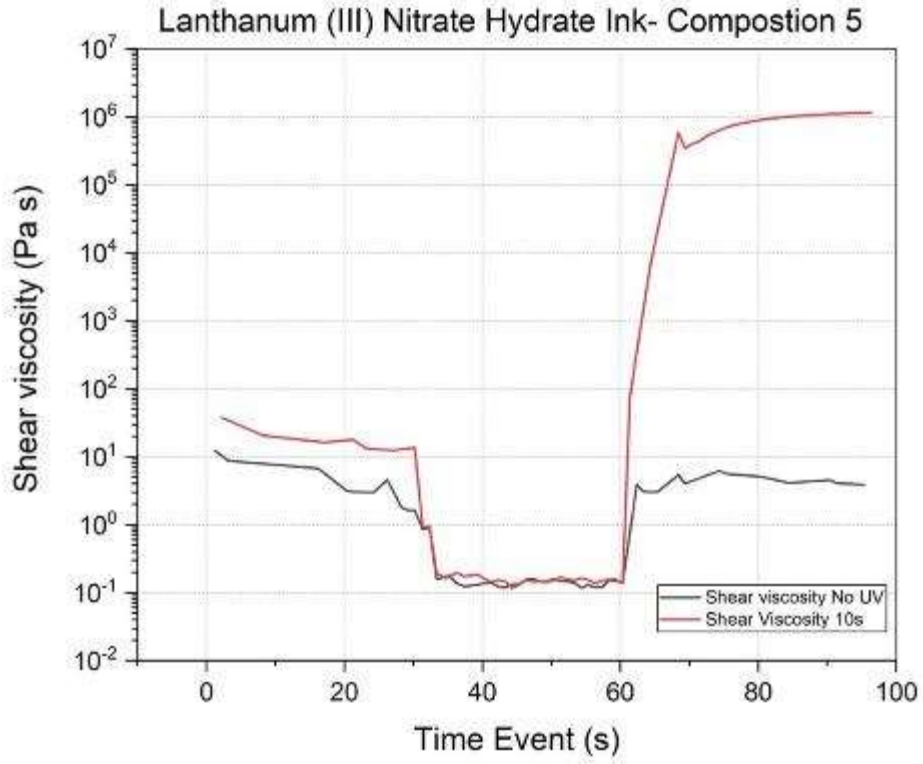

Figure 3.5. Three steps profile test for composition 5 of lanthanum nitrate ink.

3.3 Hybrid technology

Hybrid equipment was described in paragraph §2.3 (Figure 2.2): it consists in positioning UV-LEDs spotlights around the nozzle by considering the following inverse relation ($I \alpha d^{-2}$). The hexagonal ring consists of 5 spotlights at distance of ~ 20mm from the nozzle and at an angle of 30° from the printing base. This arrangement ensures that the component during printing is not damaged and allows adequate light intensity to easily cross-link the filament (20).

For both compositions, the fourth for cerium nitrate and the fifth for lanthanum nitrate, two printing components were obtained in relation to their rheology as already reported in paragraph 3.4.2 (Figure 3.6 and 3.7).

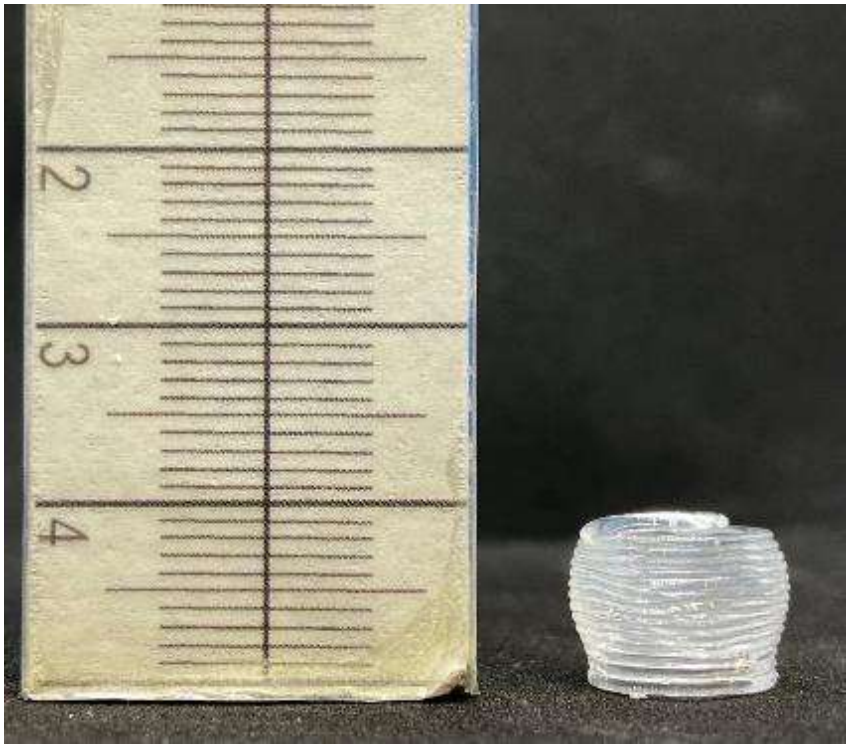

Figure 3.6. Printed sample of composition 4 of Cerium Ink after sintering at 1400°C for 5 min.

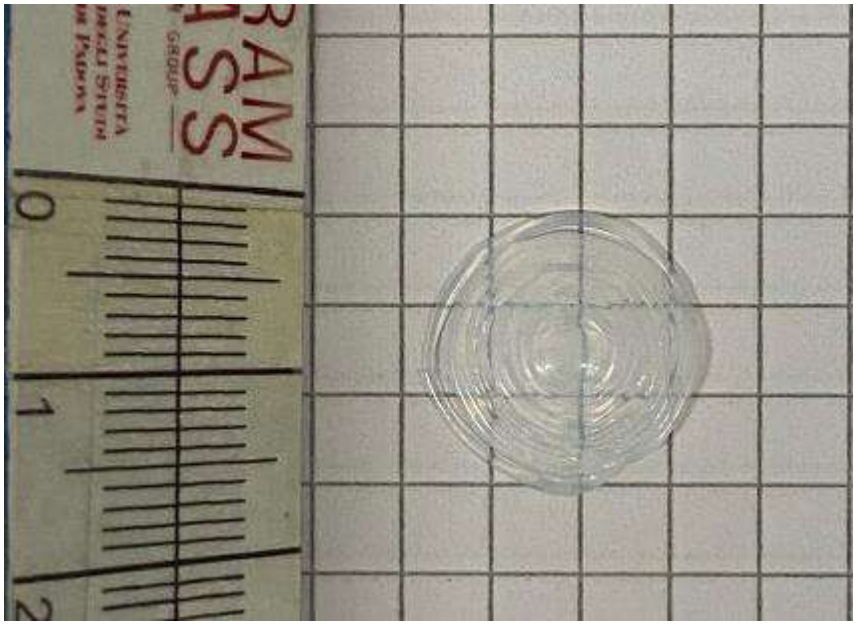

Figure 3.7. Printed sample of composition 5 of Lanthanum Ink after sintering at 1400°C for 5 min.

The components were obtained by tailoring extrusion so that the speed of the printing head matches the speed of the ink flowing through the tip; moreover, if the speed is too high the filament may break, if it is too slow it can cause excessive ink to leak. The rigidity of the component is given by photopolymerization thanks to the presence of UV-LEDs light that

allows the component to reticulate. The required energy for photo crosslinking depends on the intensity light, the time of exposure and to extrusion speed: if the latter is too slow, it can cause the cross-linking of the material directly on the tip of the extruder. An optimal speed range that serves as a good compromise for good printing was found between 7-10 mm/s.

Figure 3.6 shows a printed component, a small vase with a height of $\sim 1\ cm$, at 7 mm/s with a 580nm tip nozzle; there is good resemblance of the model file. The flow has been regulated by setting a pressure of 1.2 bar. Figure 3.7 shows a printed component, a spiral with a $\phi \sim 1.5\ cm$, at 10 mm/s with a 580nm tip nozzle. The extrusion pressure, regulated always during printing, is about 0.4 bar.

It's possible to see from both images that the structures for the two inks are different: the low viscosity of lanthanum ink compared to cerium ink allowed the printing of a single layer component.

Figures 3.6 and 3.7 show the samples after sintering; in the process, they have retained their original shapes. The samples are well densified after treatment and appear crack-free: this confirms that the treatment at 1400°C for 5min is the most effective and allows to keep transparent samples.

3.4 Heating treatments

In the paragraph §2.5, heating treatments are described: the first is debinding and the second is sintering. Debinding is the most important step but at the same time the most critical and the slowest. This treatment allows to eliminate the organic part completely but gradually, leaving a highly porous green body of silica. The various steps involve the condensation of TEOS at 160°C, the decomposition of acrylates (which is maximum at 200°C and at 350°C) and the total removal of -OH groups from silica particle surface (at 800°C). The duration of treatment is short (23h) compared to the most common debinding times that require even more days: it is due to the addition of TEOS which acts as silica source limiting the amount of organic to be removed (20) (29).

After the debinding, samples are ready for sintering process. Sintering temperatures and times are collected in Table 2.4. During sintering, the highly porous samples are transformed in transparent glass by the process of viscous sintering which permits to eliminate pores and to densify green bodies. One important factor which leads to densification is the reduction of surface particle free energy, which is the driving force for sintering. (30). In this mono-component system, however, the presence of TEOS in green bodies can help in reducing the energy requirements and thus the sintering temperature thanks to its amorphous nature; a

residual number of hydroxy groups in silica particles may play a role in the hydrolysis of TEOS, which its subsequential condensation on silica particles surfaces. This can lead to siloxane bridges formation between adjacent particles and a good densification also at lower temperatures. (31)

It is important, during sintering, to consider the role of the metal oxide precursors. For example, the addition of lanthanum nitrate within the silica matrix can result in higher porosity: in fact, lanthanides have been used to produce porous silica materials for solid oxide fuel cells, thanks to their high ionic conductivity at low temperatures. Materials exhibited a large increase in pore size distribution by forming a lanthanum silicate phases ($La_{9.33}Si_6O_{26}$). To avoid macroporosity, the concentration of lanthanum must be kept at a ratio La/Si below 1.5. (32) In fact, between the five different compositions of lanthanum inks reported in paragraph 2.1, only from the fifth composition transparent samples are obtained. This because the ratio of La/Si is less than 1.5 (0.113) (Figure 3.8). By reducing the macroporosity, dense glass sample can be obtained.

Figure 3.8. A dense sample of lanthanum ink, composition 5.

For Cerium (III) Nitrate Inks, cerium concentration improves the material densification: for example, in a sol-gel silica network, cerium ions are located by replacing H+ ions in silanol groups (≡Si–OH). Once green bodies are densified, cerium ions can be coordinated by six or more oxygen atoms to satisfy electroneutrality of glass network. If concentration of Cerium increases, a more closed and interconnected structure can form. (33).

However, by considering the various compositions of cerium ink, reported in paragraph §2.1, a concentration greater than 0,10 wt% of cerium in mixture can lead a pigmentation of post-sintering samples without obtain transparent samples (Figure 3.9 - 3.10 - 3.11).

The last important parameter is sintering time: by increasing sintering time, samples can bloat and crack compromising their densification and transparency (Figure 3.12 – 3.13). Therefore, samples were kept at 1400°C only for 5 minutes. In this way, samples can obtain a higher value of density than other samples sinter for much more time.

Figure 3.9. A sample of composition 1 of cerium ink after sintering.

Figure 3.10. A sample of composition 2 of cerium ink after sintering.

Figure 3.11. A sample of composition 4 of cerium ink which obtain a transparent sample after sintering.

Figure 3.12. A sample of composition 1 of Lanthanum ink after sintering at 1350°C for 30 min.

Figure 3.13. A sample of composition 2 of Cerium ink after sintering at 1400°C for 30 min.

3.5 Density and porosity measurements

After sintering process, density and porosity of various samples were measured. Their values are collected in the following table.

Table 3.1. Temperature and time of sintering for Lanthanum (III) Nitrate Hydrate inks.

Composition	Sintering temperature [°C]	Sintering time [s]	Density $[g/cm^3]$	Porosity [%]
1	1400	5	1.72	4.52
		10	1.69	4.78
		15	1.67	5.20
	1350	15	1.67	5.21
		30	1.66	5.38
		60	1.63	6.62
2	1400	5	1.74	3.82
		10	1.73	3.84
		15	1.72	3.86
	1350	15	1.70	4.71
		30	1.69	4.77
		60	1.66	4.78
3	1400	5	1.81	3.79
		10	1.8	3.81
		15	1.79	3.82
	1350	15	1.78	4.2
		30	1.76	4.42
		60	1.71	4.58
4	1400	5	1.89	2.80
		10	1.87	3.2

		15	1.86	3.5
	1350	15	1.78	4.18
		30	1.73	4.46
		60	1.72	4.47
5	1400	5	2.19	0.053
		10	2.17	0.089
		15	2.17	0.089
	1350	15	2.08	0.12
		30	2.06	0.15
		60	2.06	0.15

Table 3.2. Temperature and time of sintering for Cerium (III) Nitrate Hexahydrate inks.

Composition	**Sintering temperature [°C]**	**Sintering time [s]**	**Density $[g/cm^3]$**	**Porosity [%]**
1	1400	5	1.28	14.8
		10	1.26	15.0
		15	1.20	16.8
	1350	15	1.19	17
		30	1.17	19
		60	1.17	20
2	1400	5	1.53	7.6
		10	1.52	7.8
		15	1.51	7.7

	1350	15	1.47	8.2
		30	1.45	8.4
		60	1.45	8.5
3	1400	5	2.10	1.03
		10	2.09	1.07
		15	2.07	1.11
	1350	15	2.05	1.20
		30	2.04	1.21
		60	2.02	1.23
4	1400	5	2.20	0.040
		10	2.19	0.052
		15	2.19	0.053
	1350	15	2.17	0.073
		30	2.15	0.079
		60	2.13	0.090

As reported in the Table 3.1 and 3.2, it is possible to notice that as sintering time increases, density decreases and porosity increases. As mentioned, increasing sintering times might have led to bloating and the formation of cracks and, consequently, to a decrease of density. In addition, it is possible to note that, between the two sintering temperatures, the lower one shows the lowest density values: this is probably due to the fact that this temperature is too low to favor a complete sintering in the given time window (see paragraph §3.4). The best results were obtained at 1400°C for 5 min, both for lanthanum and cerium samples: both temperature and time are the right compromise between a complete sintering and a good surface integrity. The best results were obtained for the two optimized inks, respectively the composition 5 of lanthanum and the composition 4 of cerium, whose density values are close to silica glass

density (2.2 g/cm^3) which is unchanged although both precursors have higher densities (2.4g/cm^3 for lanthanum and for cerium 2.4g/cm^3) (34). It is also visible from the following graphs, which report density values for each lanthanum and cerium inks by changing temperature and sintering time. As already mentioned, the best treatment that allows to obtain dense samples is at 1400°C for 5 min for both precursors, respectively cerium and lanthanum. (Figures 3.14, 3.15)

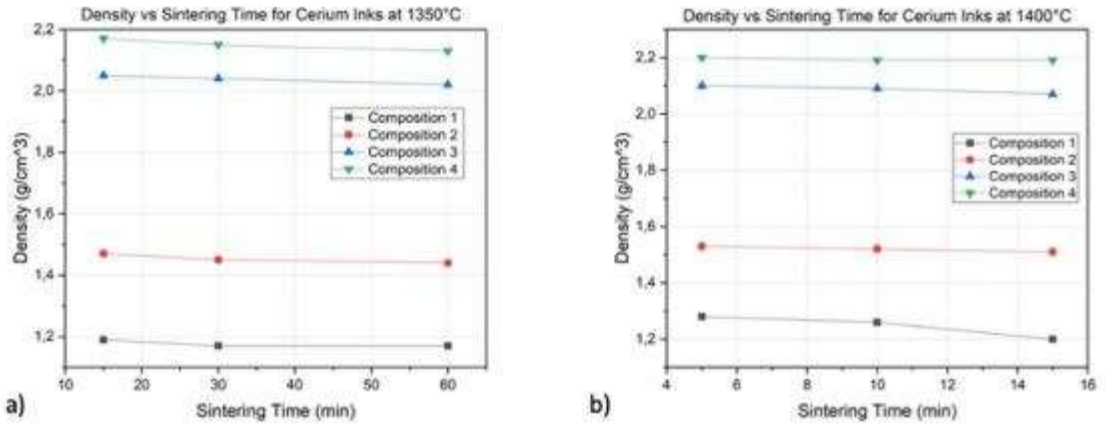

Figure 3.14. Density of cerium nitrate inks a) at 1350°C; b) at 1400°C.

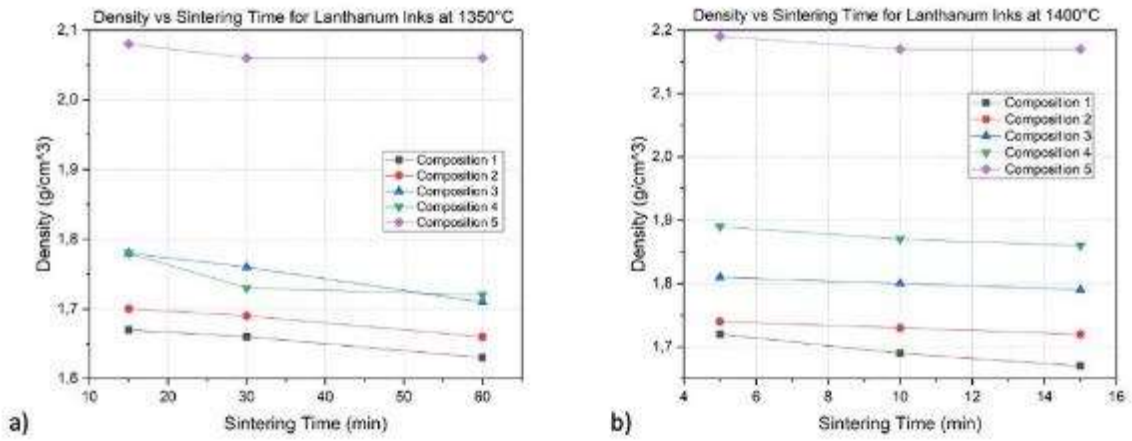

Figure 3.15. Density of lanthanum nitrate inks a) at 1350°C; b) at 1400°C.

3.6 Optical measurements

The next paragraphs focus on spectrophotometric analysis of cerium samples and refractometric measure of lanthanum samples, to verify respectively photoluminescence and the refractive index.

3.6.1 Spectrophotometric analysis

Photoluminescent glasses have important role in white light emission, laser generation and optical temperature sensing (29). Cerium enhances the photo-luminescence properties of silica glass when irradiated with UV light, it converts it into the visible range thus emitting a blue light. The emission spectra of the doped glass under excitation at 280 nm was measured with a spectrophotometer. The photoluminescent photo was taken by a phone in a dark room under the illumination of a 280 UV lamp.

Silica glass samples look the same under natural light because cerium ions do not have intense absorption in the visible range due to their low concentration (Figure 3.16), but their emission is distinguishable by eyes under the excitation of a 280 nm lamp. (Figure 3.17).

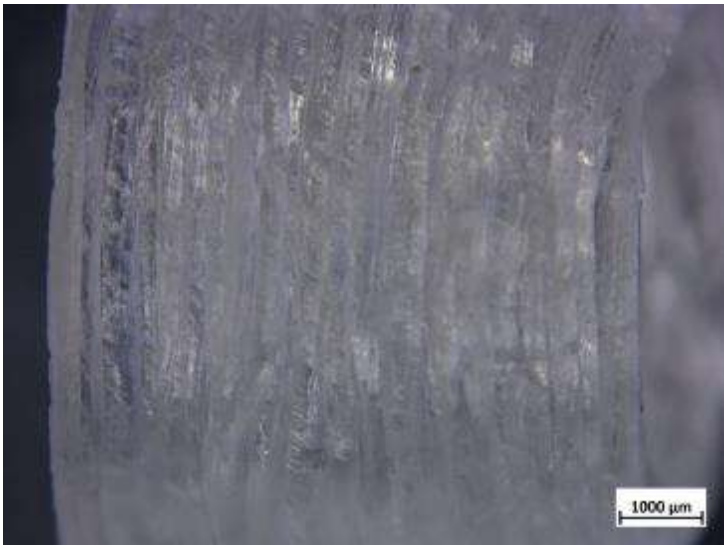

Figure 3.16. An image of a cerium sample without UV lamp irradiation.

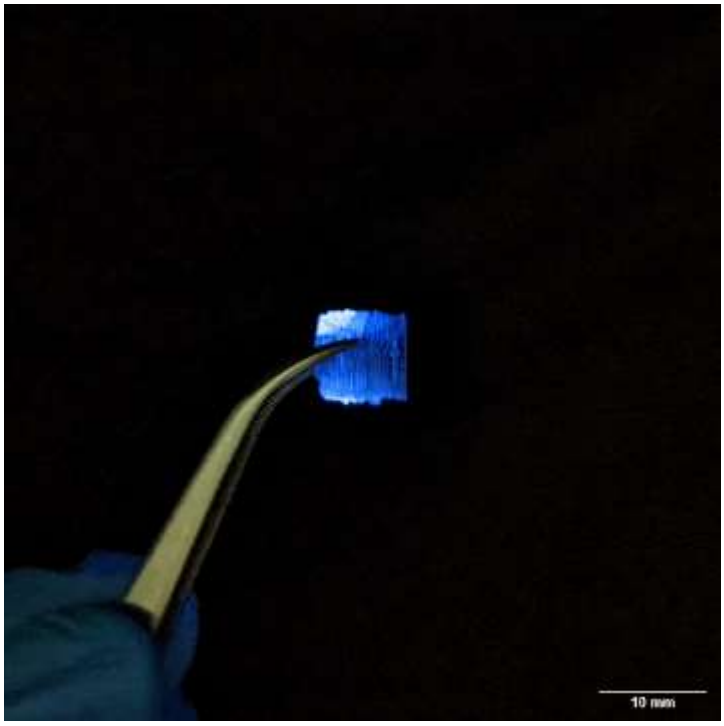

Figure 3.17. An image of a cerium sample with UV lamp irradiation.

In Figure 3.18 the emission peak of Ce^{3+} doped silica glass at 350-550 nm is due to the 5d → 4f transition of Ce^{3+} ions (29). Obviously, the peak position and its underlying area depend on how much silica glass has been doped, so the graph is only relative to the case studied in the thesis.

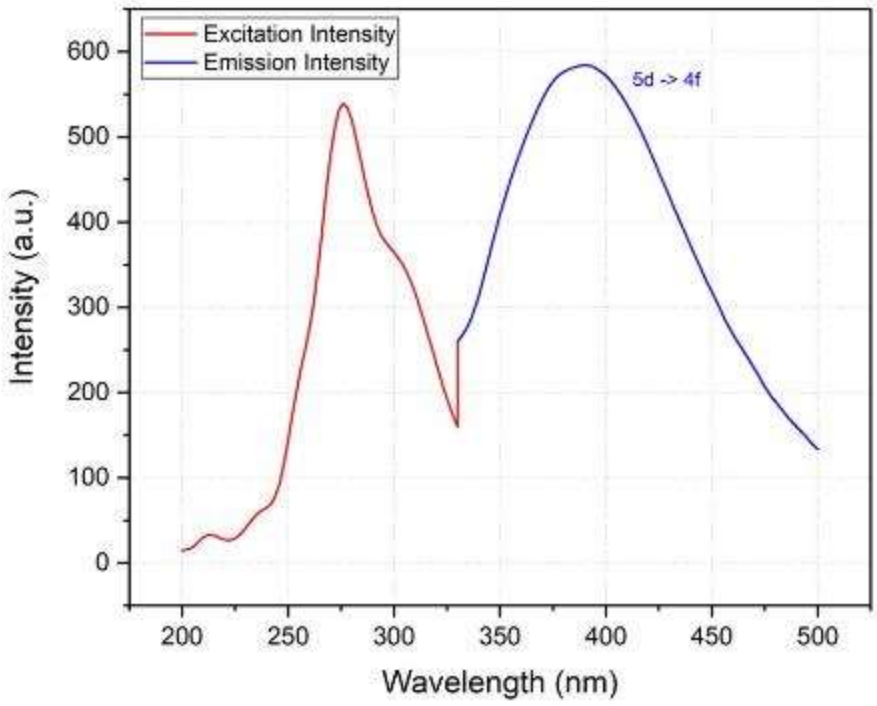

Figure 3.18. Absorbance and emission spectra of cerium nitrate sample from composition 4.

3.6.2 Refractive index measurement

From the measure of the lanthanum sample, a refractive index value of 1.629 was obtained: this value is higher than that of a pure silica glass, which has an index of 1.453, therefore confirming that the glass composition was modified correctly. This increase is due to the optical property of lanthanum: it is based on the phenomena of absorption in the visible range and with the consequently transition in the orbital 4f of La^{3+} ions. (5)

It is also possible to state that by increasing sample densification and by reducing residual porosity, scattering is reduced by increasing the refractive index.

Chapter 4

Conclusion

4.1 Conclusions

A new hybrid technology has been adopted for the printing of multi-component silica glass: this technology originates from the combination of DLP and DIW. This new technology allows to fabricate freeform structures, which would be difficult to obtain with the most common methods of glass making. This is possible thanks to the combination of DIW technology that permits to obtain more complex structures and the use of UV-LEDs light that allow the printed object obtained by DIW not to collapse on itself and to maintain the shape corresponding to the digital CAD model.

Obviously, this type of printing still requires some tailoring of the rheological properties of the inks: as already reported in paragraph §3.4, the ink must have a pseudoplastic behavior so that the ink can be extruded without problems and that it maintains the desired shape once extruded. Moreover, it must be reactive to UV light: this reactivity is increased by the fact that most of components ink have the same refractive index. This was verified by the three steps profile test, which confirmed the increase of the ink rigidity upon irradiation by UV light.

The stability of the inks was achieved despite the addition of oxide precursors, respectively Cerium (III) Nitrate Hexahydrate and Lanthanum (III) Nitrate Hydrate, which in the right percentages by weight did not adversely affect both base silica mixture and its reactivity to UV light.

The final composition of cerium glass, SiO_2:Ce_2O_3 = 99.8:0.2,allowed to obtain an ink with adequate rheological properties characterized by a shear thinning behavior: this has made it possible to obtain 3D prints, which faithfully reflect CAD model. Dense and transparent glass samples were obtained, which have been shown to possess good photoluminescent properties as confirmed by spectrophotometric measurements.

The final composition for lanthanum glass, SiO_2:La_2O_3 = 91.2:8.8 , a pseudoplastic behavior, yet much weaker: this ink permitted to obtain fewer complex prints than cerium. In any case,

dense and transparent samples were obtained after sintering. They also demonstrated good optical properties, confirmed by refractometric analysis, which reported an increase in the silica-based glass remarking index from 1.453 to 1.629.

4.1.1 Future perspectives

Despite the good results obtained, it is however important to deepen the study concerning the multicomponent inks.

As for cerium ink, more complex shapes could be printed by optimizing the ink formulation; for example, by tailoring the TEGDA/HEMA ratio it could be possible not only to increase the viscosity of the ink, but especially its reactivity, therefore increasing its free-forming ability.

Such optimization represent a possible solution of the poor viscosity showed by the La-based formulation. In addition, other refractometric measurements should be repeated on other samples, to have further confirmation of the actual increase in the refractive index.

Moreover, for both inks it will be necessary to measure the percentage transmittance.

References

1. Du T. Nguyen, Cameron Meyers, Timothy D.Yee,Nikola A. Dudukovic, Joel f. Destino, Cheng Zhu, Eric B. Duoss, Theodore F. Baumann, Tayyab Suratwala, James E.Smay and Rebecca Dylla-Spears. *3D- Printed Transparent Glass.* United States : Advanced Materials, 2010.

2. Fanderlik, I. *Silica Glass and its applications.* Prague : ELSEVIER, 1991.

3. D.R, Uhlmann and N.J. Kreidl, eds. *Optical Properties Of Glass.* United States : The American Ceramic Society, 1991.

4. Chang Liu, Bin Qian, Rongping Ni, Xiaofeng Liu and Jianrong Qiu. *3D printing of multicolor luminescent glass.* s.l. : Royal Society of chemistry, 2018.

5. L.W.RIKER. *The Use of Rare earths in Glass Compositions.* United States : s.n., 1981.

6. H.Scholze. *Glass, Nature, Structure and Properties.* s.l. : Springer-Verlag, 1991.

7. Rasmussen, Seth C. *A Brief History of Early Silica Glass: Impact on Science and Society.* s.l. : Substantia , 2019.

8. Britannica. *History of glassmaking-Devolopment of the glassmaker's art, https://www.britannica.com/topic/glass-properties-composition-and-industrial-production-234890/History-of-glassmaking.*

9. W. Höland, G. Beall. *Glass Ceramics Technology.* s.l. : he American Ceramic Society, 2002.

10. G.Scarinci, T. Toninato, B.Locardi. *Vetri.* s.l. : Ambrosiana , 1977.

11. Colombo, Paolo. *Technology of sheet and container glass.*

12. Team, Triditive. *What is additive manufacturing? History and benefits.* April 4, 2022.

13. KLEIN, JOHN. *ADDITIVE MANUFACTURING OF OPTICALLY TRANSPARENT GLASS.* September 2015.

14. Reda Mohammed Zaki, Clément Strutynski, Simon Kaser, Dominique Bernard, Gregory Hauss, Matthieu Faessel, Jocelyn Sabatier, Lionel Canioni, Younès Messaddeq , Sylvain Danto, Thierry Cardinal. *Direct 3D-printing of phosphate glass by fused deposition modeling.* s.l. : ELSEVIER, 2020.

15. John Klein, Michael Stern, Giorgia Franchin, Markus Kayser, Chikara Inamura, Shreya Dave, James C. Weaver, Peter Houk, Paolo Colombo, Maria Yang and Neri Oxman. *Additive Manufacturing of Optically Transparent Glass.*

16. Andrea Alice Konta, Marta Garcia, Dolores R. Serrano. *Personalised 3D Printed Medicines: Which Techniques and Polymers Are More Successful?, DOI: 10.3390/bioengineering4040079.* 2017.

17. print, Filament 2. *https://filament2print.com/gb/filament-fdm/1472-artillery-hornet-fdm-3d-printer.html.*

18. Du T. Nguyen, Cameron Meyers, Timothy D. Yee, Nikola A. Dudukovic, Joel F. Destino, Cheng Zhu, Eric B. Duoss, Theodore F. Baumann, Tayyab Suratwala, James E. Smay, and Rebecca Dylla-Spears. *3D-printed Transparent Glass.* s.l. : WILEY-VCH , 2017.

19. Shaheryar Atta Khan, Ismail Lazoglu. *Development of additively manufacturable and electrically conductive graphite–polymer composites.* s.l. : Springer, 2020.

20. Anna De Marzi, Giulio Giometti, Johannes Erler, Paolo Colombo, Giorgia Franchin. *Hybrid additive manufacturing for the fabrication of freeform transparent silica glass components.* s.l. : ELSEVIER, 2022.

21. S.Tagliaferri, A. Panagiotopoulos and C.Mattevi. *Direct ink writing of energy materials.* s.l. : Royal society of chemistry, 2020.

22. Andrea Zocca, Giorgia Franchin,Paolo Colombo, Jens Gunster. *Additive Manufacturing.* s.l. : Elsevier , 2020.

23. A. Davoudinejad, A. K. Jessena, S. D. Farahani , N. Frankec, D. B. Pedersena, G. Tosello. *Geometrical shape assessment of additively manufactured features by Continuous Liquid Interface Production vat photopolymerization method.* Denmark : s.n., 2019.

24. Peng Cai, Liang Guo, Hao Wang, Jiaming Li, Jintao Li, Yixin Qiu, Qingmao Zhang, Qitao Lu. *Effects of slurry mixing methods and solid loading on 3D printed silica glass parts based on DLP stereolithography.* s.l. : Elsevier, 2020.

25. *Ultraviolet-Assisted Direct-Write Fabrication of Carbon Nanotube/Polymer Nanocomposite Microcoils.* Lebel, Louis Laberge, et al. 2010, Advanced Materials, Vol. 22, pp. 592-596.

26. Berger, M B. *THE IMPORTANCE AND TESTING OF DENSITY / POROSITY / PERMEABILITY / PORE SIZE FOR REFRACTORIES.* 2010.

27. [Online] Aldrich, Sigma. https://www.sigmaaldrich.com/IT/it/substance/lanthanumiiinitratehexahydrate4330110277437.

28. J. Rubio-Hern´andez, J.H. S´anchez-Toro, N.M. Pa´ez-Flor. *esting shear thinning/ thixotropy and shear thickening/antithixotropy relationships in a fumed silica suspension.* s.l. : J. Rheol, 2020.

29. Chang Liu, Bin Qian, Xiaofeng Liu, Limin Tong and Jianrong Qiu. *Additive manufacturing of silica glass using laser stereolithography with a top-down approch and fast debinding.* s.l. : Royal Society of Chemistry, 2018.

30. Arnaud Ndayishimiye, Alain Largeteau, Stéphane Mornet, Mathieu Duttine, Marie-Anne Dourges, Dominique Denux, Marc Verdier, Mohamed Gouné, Thomas Hérisson de Beauvoir, Catherine Elissalde, et al. *Hydrothermal sintering for densification of silica. Evidence for the role of water.* s.l. : ELSEVIER, 5 March 2021.

31. Arnaud Ndayishimiyea, b,∗, Kosuke Tsuji, Ke Wanga, Sun Hwi Banga, Clive A. Randalla. *Sintering mechanisms and dielectric properties of cold sintered (1-x) SiO2 - x PTFE composite.* s.l. : Journal of the European Ceramic Society, 29 July 2019.

32. Benjamin Ballinger, Julius Motuzas, Christopher R. Miller, Simon Smart & Joa˜o C. Diniz da Costa. *Nanoscale assembly of lanthanum silica with dense and porous interfacial structures.* Australia : s.n., 3 february 2015.

33. M. Garcia-Heras a, A. Jimenez-Morales, B. Casal, J.C. Galvan, S. Radzki, M.A. Villegas. *Preparation and electrochemical study of cerium–silica sol–gel thin films.* s.l. : ELSEVIER, 2004.

34. Yongsheng Han, Jian Bao Li, Bo Chi, Zhong He Wen. *The Effect of Sintering Temperature on Porous Silica Composite Strength.* s.l. : Journal of Porous Materials, March 2003.

35. Jacobs, P.F. *Rapid Prototyping & Manufacturing: Fundamentals of StereoLithography.* s.l. : American Society of Mechanical Engineers, ASME, 1992.

36. Anuraag Gaddam, Hugo R. Fernandes, Dilshat U. Tulyaganov, José M.F. Ferreira. *The structural role of lanthanum oxide in silicate glasses.* s.l. : ELSEVIER, 2018.

37. Nalwa, Hari Singh. *The refractive index of silica glass and its dependence on pressure, temperature, and the wavelength of the incident light.* United States : ACADEMIC PRESS, 2001.

38. MICROSCOPES, OPTIKA. *Operation MANUAL-https://www.manualslib.com/manual/1530433/Optika-2waj.html#manual.* Italy : s.n.

39. M. Wozniak, T. Graule, Y. de Hazan, D. Kata, J. Lis. *Highly loaded UV curable nanosilica dispersions for rapid prototyping applications,.* s.l. : J. Eur. Ceram. Soc. , 2009.

40. M. deLombard-Watts, P.T. Weissman. *Comparison of performance of acrylate and methacrylate aliphatic urethanes.* s.l. : RadTech Tech. Proc, 2004.

41. S.R. Raghavan, H.J. Walls, S.A. Khan. *Rheology of silica dispersions in organic liquids: new evidence for solvation forces dictated by hydrogen bonding.* s.l. : Langmuir 16 , 2000.

Acknowledgements

First, I would like to thank Professor Giorgia Franchin for giving me the opportunity to work on this project.

Thanks also to engineer Anna De Marzi for always helping and following me.

Thanks to my parents for their constant dedication, for their endless support during this university path.

A special thanks to my boyfriend, Matteo, for always encouraging me.

Thanks to Alice and Michele for their special friendship.

Thanks to my lab mates for the beautiful moments spent together.

A huge thanks to my life friends: Alessia, Giada and Davide. Thanks for making me smile even in the darkest moments.

And finally, I would like to thank the most important person of my life, my granny Erminia. This thesis is dedicated to her as a thank for having completely dedicated herself to me in her last years of life. If I made it today, it is because of her.